A Structural X-ray Study on Semifluorinated Alkanes (SFA): SFA Revisited

P. Marczuk and P. Lang*

Iwan-N.-Stranski-Institut für Physikalische und Theoretische Chemie, Technische Universität Berlin, Strasse des 17, Juni 112, D-10623 Berlin, Germany

Received July 17, 1998; Revised Manuscript Received October 5, 1998

ABSTRACT: We present an X-ray scattering study on a series of semifluorinated *n*-alkane ($F_{12}H_n$) powder samples, with even−numbered hydrocarbon chains $n = 6-18$. At elevated temperatures the samples appear to have a simple lamellar structure consisting of single-layered stacks. At ambient temperature three different rather complex bulk structures were observed as a function of the chain length of the hydrocarbon molecular moiety. Our results are compared to structure models for $F_{12}H_n$ found in the literature, and some new features of the structure of the room temperature phase are disclosed.

Introduction

Semifluorinated alkanes (SFA) with the general chemical structure $F(CF_2)_m(CH_2)_nH$ abbreviated F_mH_n have gained increased scientific attention since the 1980s in a 2-fold way. On the one hand, SFA molecules can be regarded as a linkage of two parts (alkyl and perfluoroalkyl) which, as a matter of principle, are only poorly miscible with each other,[1,2] thus exhibiting amphiphilic character and consequently having a high tendency to self-organization and a certain surface activity. They form liquid-crystalline phases,[3−5] adsorb at the hydrocarbon/air interface,[6,7] and aggregate when dissolved in apolar solvents.[8,9] It was argued that SFAs could be regarded as a novel class of structurally simple model surfactants because its alkane solutions are of much greater simplicity in terms of interaction forces than conventional water/surfactant systems. On the other hand, SFAs have been extensively investigated[10,11] as they had been regarded as short−chain model compounds for the infinite-chain analogues ($-(CF_2)_m-(CH_2-)_n$), which are expected to combine the advantageous thermal stability of poly(tetrafluoroethylene) (PTFE) and the processability of polyethylene. Numerous publications concerning the structure of semifluorinated alkanes[3−5,10−12,14] in the solid or liquid-crystalline state present as results a great variety of packing structures due to the mutual incomensurability of the fluorinated and the hydrogenated segments.

For the qualitative interpretation of the diffraction data, it is useful to recall the structure of the pure alkane and perfluoroalkane compounds in the solid state. *n*−Alkanes are known to pass through several solid modifications between room temperature and their melting points, and all phase transitions can be associated with the onset of a characteristic motion.[19] In the low-temperature phases the planar "zig-zag" carbon backbones are arranged in layers of triclinic or orthorhombic unit cells, and as thermal motion increases, the so-called "rotator phases" are formed. The latter term describes layered phases with hexagonal symmetry originating from a superposition of rotational, translational, and conformational disorder in the samples.[20] Perfluoro-*n*-alkanes are known to undergo solid−solid phase transitions in a similar manner.[21] However, their intramolecular structure is a little different. Because the van der Waals radius of fluorine atoms is larger than half the *C*−*C* distance, steric hindrance causes the chain to prefer a 15/7 helical conformation, attributing rigidity to the carbon backbone and enlarging the cross-sectional area from 18.5 to 28.3 Å^2,[16,18] with a hexagonal arrangement being assumed.

If the results from the above-mentioned studies on *n*−alkanes and perfluoro−*n*−alkanes are combined, one gets an idea of the length l_e of a $F_{12}H_n$ molecule:[16,17]

$$l_e = (1.67 + n \times 0.1265 + 0.15)\ \text{Å} \qquad (1)$$

where 1.67 Å is the length of the F_{12} segment (l_F) and accordingly the length of the hydrogenated part is given by $l_H = l_e - l_F$.

In this contribution we present a detailed small-angle X-ray scattering (SAXS) study on powder samples of the homologue series $F_{12}H_n$, with *n* being an even number of carbon atoms ranging from 6 to 18. The short-chain members of this group with $n \leq 14$ are known to undergo a solid/solid phase transition below their melting point, i.e., in the temperature range from 316 K for $F_{12}H_6$ to 363 K for $F_{12}H_{14}$. On the basis of thermal analysis data,[13] this transition was attributed to a disordering of the hydrocarbon chains only. On the other hand, SAXS experiments by Rabolt et al.[10,11] showed that the solid/solid phase transition manifests itself in a complete structural reorientation of the samples. In the high-temperature phase all compounds with $n \leq 14$ were reported to cause SAXS spectra consisting of one single peak, with the corresponding *d* spacing matching the molecular length of the respective $F_{12}H_n$ molecule. This was interpreted to be strong evidence for a simple lamellar structure with molecular monolayers as the repeating motive.

In the low-temperature phase the experimental findings can be categorized into three groups.[11] For $n \leq 6$ there is only one peak in the SAXS curves observed corresponding to a lattice spacing which is equal to or slightly less than the fully extended molecular length. The ambient-temperature spectra from the samples with $8 \leq n \leq 12$ were previously interpreted in terms of a coexistence of the high-temperature phase with the low-temperature phase. The curves were reported to consist of the first- and second-order peaks originating from the low-temperature phase plus an additional first-

10.1021/ma981130j CCC: $15.00
Published on Web 12/01/1998

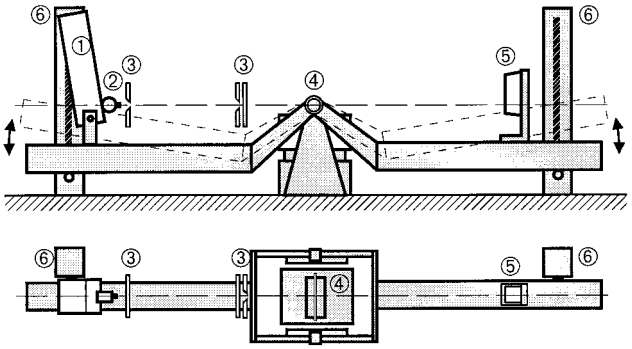

Figure 1. Side view (above) and top view (below) of the experimental setup for SAXS and WAXD measurements: (1) X-ray tube; (2) graphite monochromator; (3) slits; (4) sample; (5) position-sensitive detector; (6) vertical stages. This setup allows the observation of SAXS and WAXD data up to a scattering angle of 22°.

order peak reminiscent of the high-temperature phase. The spacings from the dominant low-temperature phase were found to be proportional to the length of the alkane chain plus twice the length of the perfluorinated segment. At ambient temperature the reported long period from the samples with $n \geq 14$ increases sharply with the hydrocarbon chain length and is somewhat less than twice the molecular length.

In the present paper we also report on SAXS experiments from $F_{12}H_n$ powder samples, which qualitatively confirm the experimental data by Rabolt et al. However, since the former studies were conducted with a Kratky camera using a slit-collimated primary beam, the data suffer from a lack of resolution. Consequently, important details of the observed structures could not be deduced from the beam profile smeared data. This paper is meant to add some of these details to the collection of data on SFAs although we are not in the position to present a thorough analysis of all of the structural details of pure SFAs in their different solid (or rather liquid-crystalline) phases.

Experimental Section

Materials. The SFA samples were put at our disposal by the group of Prof. M. Möller at University of Ulm, Ulm, Germany, where the samples had been synthesized and purified according to the method of Höpken et al.[13,14] Samples with an impurity content above 2% had been further purified by sublimation.

SAXS. SAXS data were collected on a home-built instrument which was originally designed to carry out reflectivity measurements (see Figure 1). The instrument is equipped with a standard Cu tube as the X-ray source and was operated at 40 kV and 35 mA. A graphite monochromator (type 151, Huber Diffraktionstechnik, Rimstig) was used to select the Cu Kα wavelength ($\lambda = 0.1542$ nm). The collimating system consisted of one vertical and two horizontal slits (type 3012, Huber) limiting the incident beam's cross section to a square of 0.25×0.25 mm^2. The scattered radiation was discriminated electronically, and detection was made by a Braun OED-50M metal wire position-sensitive detector (PSD) of 50 mm active length attached vertically for all SAXS measurements. All optical components were mounted on two X-95 profiles which were connected by a swivel joint. For the SAXS measurements the profiles were adjusted in an angular range of $0° \leq 2\theta \leq 8°$ by means of two vertical stages (type 5101, Huber) resulting in scattering vectors of $0.5 \leq q \leq 6$ nm^{-1}, with $q = 4\pi/\lambda \sin(\theta/2)$ being the scattering vector. This setup provided simultaneous 2θ scans of approximately 8°. The accessible range of scattering vectors was easily expanded by inclining the detector arm with respect to the incident beam. Thus, wide-angle diffraction patterns up to a scattering angle of $2\theta = 22°$ were obtained as well.

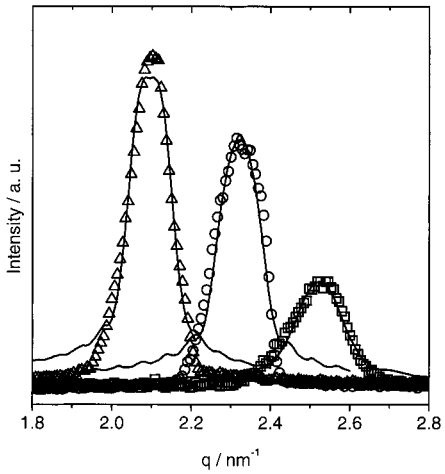

Figure 2. SAXS patterns of $F_{12}H_n$ samples at 75 °C, i.e., in the high-temperature phases. Symbols represent experimental data, and full lines are fits according to eq 4 (△, $n = 10$; ○, $n = 8$; □, $n = 6$).

Specimens were held in standard X-ray glass capillaries having a diameter of 1 mm and a wall thickness of 0.01 mm, and their distance to the detector was fixed at 324 mm. An electronic temperature controller (K−PR 70, Paar) was used to keep the temperature constant. The angular precision of the mechanical and detection systems was verified by a silver behenate powder sample,[15] and data were corrected for background scattering, detector efficiency, and glass capillary scattering.

Results and Discussion

The mentioned cross-sectional incomensurability between fluorinated and hydrogenated segments of SFA molecules is expected to affect the crystal structure. Also, one would expect influence on the crystal structure due to the mutual incompatibility of the two covalently bound parts of SFA molecules; i.e., fluorocarbon−hydrocarbon contacts should be minimized. The latter requirement leads to the first qualitative conclusion that a bilayered lamellar structure should be the most favorable for the SFAs because in such an arrangement the fluorocarbon−hydrocarbon contacts would be confined to the loci of the covalent CF_2-CH_2 bonds. Further, such a structure allows the hydrocarbon segments to interdigitate, which enables the adjustment of the lateral chain density to fill up the space available defined by the cross-sectional area of the fluorocarbon segments. Nevertheless, the SAXS data by Rabolt et al. in accordance with our data show without any doubt that in the high-temperature phase the SFAs form monolayered lamellar phases, with the long period being equal to or slightly less than the extended chain length of the molecules.

SAXS Data from the High-Temperature Phase. The temperature range accessible with our instrumentation was limited to a maximum of about 75 °C. Accordingly, we could obtain SAXS data from the high-temperature phases of $F_{12}H_n$ samples with $n = 6$, 8, and 10 which are displayed in Figure 2. The peaks in these spectra may be phenomenologically fitted by a Gaussian, and the peak position represented by the center position q_c of the Gaussian is then converted into a d spacing by Bragg's relation $d_{Bragg} = 2\pi/q_c$. As can be seen from Table 1, the d spacings resulting from this formalism are only slightly but significantly smaller

Table 1. Calculated Parameters and Experimentally Found Parameters in the High-Temperature Phase[a]

	calculated			experiment / fit				
substance	l_H	l_F	l_e	d_H	d_F	d_{Bragg}	N	ϕ
$F_{12}H_6$	0.909	1.668	2.577	0.821	1.669	2.49	23	14
$F_{12}H_8$	1.162	1.668	2.830	1.037	1.669	2.71	38	17
$F_{12}H_{10}$	1.415	1.668	3.083	1.331	1.667	3.00	39	13

[a] All lengths are listed in nanometers and the tilt angles ϕ in degrees. N is the number of layers contributing to coherent scattering in the high-temperature phase.

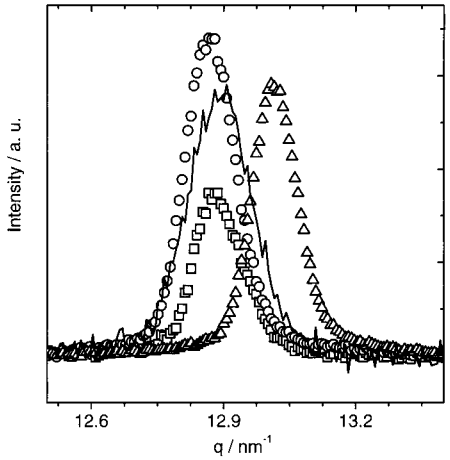

Figure 3. WAXD patterns of $F_{12}H_n$ samples (△, $n = 10$; ○, $n = 8$; □, $n = 6$) at 75 °C. For comparison the WAXD pattern from a commercial PTFE sample is also displayed (full line).

than the calculated lengths of the extended molecules (l_e). Assuming a fully elongated SFA chain and a collinear arrangement of the hydrogenated and fluorinated segment, one may calculate a tilt angle ϕ of the long molecular axis with respect to the layer normal, which is given by $\cos \phi = d_{Bragg}/l_e$. For the sample with $n = 6$, a tilt of $\phi = 14°$ results; for $F_{12}H_8$ and $F_{12}H_{10}$, the tilt angles are 17° and 13°, respectively. However, this model of a tilted arrangement is in contradiction to the wide-angle X−ray diffraction (WAXD) spectra plotted in Figure 3. All three high-temperature WAXD profiles consist of a single peak, which is strong evidence for an untilted arrangement because any inclination of the molecules would cause a more complex peak pattern. Figure 3 shows also the WAXD peak from a commercial PTFE specimen. For $F_{12}H_6$ and $F_{12}H_8$, the Bragg peak position coincides with the position of the PTFE peak, and for the sample with $n = 10$, the peak occurs at larger scattering vectors than those for the PTFE sample. This shows that the corresponding lateral distance of the SFA molecules is nearly the same for the $F_{12}H_6$ and $F_{12}H_8$ compounds, and in the case of $F_{12}H_{10}$, it is even smaller than the lateral distance of the F_n chains in the hexagonal structure of PTFE. The latter is commonly regarded as the shortest distance F_n chains can approach each other in a hexagonal arrangement.[9,14,16] We thus conclude that the WAXD spectra of the high-temperature phase are due to a structure similar to that of PTFE, i.e., a hexagonal arrangement of untilted fluorocarbon chains.

The absence of higher order Bragg peaks in the SAXS data can be explained by applying a model electron density distribution to fit the SAXS patterns. For a powder of lamellar-structured domains, it is straightforward to calculate the SAXS pattern. Since only those domains which are oriented with their layer normal parallel to the scattering vector will contribute to the diffraction, it is sufficient to calculate the Fourier transform of the electron density profile normal to the layers $\rho_e(r)$ to obtain the angular distribution of the scattered intensity:

$$I(q) = \left| \int_{-\infty}^{\infty} \rho_e(r)\, e^{iqr}\, dr \right|^2 \qquad (2)$$

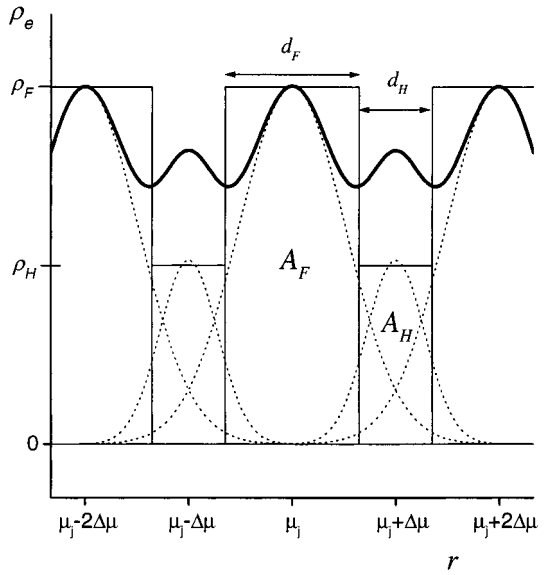

Figure 4. Model electron distribution for the lamellar high-temperature phases. Full line: the total electron density distribution normal to lamellae ($\rho(r)$) is the sum of contributions from the smeared boxes (dotted lines). Rectangular boxes represent nonsmeared slabs of fluorinated and hydrogenated sections. See text for details.

To account for translational disorder along the layer normal in the following, we used the model of smeared boxes for the electron density distribution perpendicular to the lamellae as sketched in Figure 4. The fluorinated segments of the lamellae were modeled by Gaussians, the midpoints μ_j of which were positioned at the centers of the fluorinated parts of the slabs. The area of the Gaussians representing the fluorinated moieties A_F was set to be equal to the area of the nonsmeared rectangular box (perfectly ordered molecules), and the value of the electron density at the center position of the Gaussian and that of the box ρ_F were set equal as well. This leads to the relation $d_F = \sigma_F\sqrt{2\pi}$ between the half-width at half-maximum (hwhm) σ_F of the Gaussian and the width d_F of the rectangular box. The same formalism was applied to describe the hydrogenated segments of the lamellae; however, the Gaussians representing hydrocarbon moieties were positioned at $\mu_j + \Delta\mu$. The final form of this lamellar model profile is

$$\rho_e(r) = \sum_{j=1}^{N} \frac{A_F}{\sigma_F\sqrt{2\pi}} \exp\left\{ -\frac{(r-\mu_j)^2}{2\sigma_F^2} \right\} + \frac{A_H}{\sigma_H\sqrt{2\pi}} \exp\left\{ -\frac{(r-(\mu_j+\Delta\mu))^2}{2\sigma_H^2} \right\} \qquad (3)$$

where N is the number of the lamellae which contribute coherently to the scattering, and the scattered intensity eventually reads as

$$I(q) = |F_k \sum_{j=1}^{N} \exp\{iq\mu_j\} + H_k \sum_{j=1}^{N} \exp\{iq(\mu_j + \Delta\mu)\}|^2 \quad (4)$$

with

$$F_k = A_F \exp\left\{-\frac{q^2\sigma_F^2}{2}\right\} \quad \text{and} \quad H_k = A_H \exp\left\{-\frac{q^2\sigma_H^2}{2}\right\}$$

The parameters σ_F and σ_H which are related to the thickness of the fluorinated and hydrogenated layers d_F and d_H, respectively, and N were obtained from nonlinear least-squares fits of eq 4 to the experimental data. The fitting procedure involved two steps: during the first step σ_F was held fixed at 1.67 nm to obtain a set of starting parameters for the second step where all parameters were varied. The best fits are displayed in Figure 2, and the corresponding fit parameter values are listed in Table 1. The values of the electron densities which were also obtained from the fitting procedure are physically meaningless, since we did not measure intensities on an absolute scale. It is obvious from the data in Table 1 that the values obtained for d_F match perfectly with the length of the fluorinated segment $l_F = 1.67$ nm and that the sum of d_F plus d_H is smaller than the lengths of the fully extended chains in accordance with the Bragg spacings calculated from the phenomenological fit of the SAXS peak with a single Gaussian. This confirms basically the assumption of a monolayered lamellar structure already suggested by Russell et al. However, our analysis of the SAXS data in combination with the WAXD results shows undoubtedly that the fluorocarbon segments stand upright on the lamellar planes. The measured d spacings, which are smaller than the extended chain lengths l_e, lead us to conclude that the structure in the high-temperature phase of the SFA consists of quasi-liquidlike alkane layers sandwiched between fluorocarbon layers which have a lateral structure similar to that of PTFE.

From the observed simple hexagonal unit cell it follows that no intramolecular structure details contribute to the scattering and that the molecules resemble cylindrical objects; i.e., the high-temperature phase of the $F_{12}H_n$ compounds is a rotator phase.

The number N of coherently scattering lamellae contains other important and new detailed information. N was found in all three cases to be less than or equal to 40, meaning that the samples are only weakly ordered. This explains the fact that no trace of a second-order lamellar peak is detected in the spectra of the high-temperature phases and that the whole samples have liquid-crystalline character.

SAXS Data from the Low-Temperature Phases. Compared to the SAXS data from the high-temperature phases, the spectra from the low-temperature phases exhibit a higher level of complexity, as can be seen in Figure 5. In this figure, the intensities are plotted logarithmically and the abscissa is scaled with the calculated length l_e of the molecules in order to compare the data on a qualitative level more easily. It can be seen that the spectra can be grouped into three categories with respect to the chain lengths: first, the spectrum of $F_{12}H_6$ consists mainly of three equally spaced peaks; second, the spectra of the samples with $8 \le n \le 12$ look alike in this representation; third, the spectra of the samples with $n \ge 14$ are individually different.

This classification is in line with the findings of Russell et al. However, we do not agree with their interpretation that the spectra of the samples with $8 \le n \le 12$ consist of two groups of peaks, one of which was said to be reminiscent of the high-temperature phase and the other one to consist of the first- and second-order peaks of a lamellar structure. SAXS spectra containing contributions from both the high-temperature and low-temperature phases simultaneously may actually be obtained; however, we did observe them only for $F_{12}H_6$ at ambient temperature and for the sample with $n = 8$ in the temperature range from 45 to 48 °C. We attribute the apparent coexistence of two different phases to the slow kinetics of solid/solid phase transitions, i.e., the presence of nonequilibrium states within the samples.

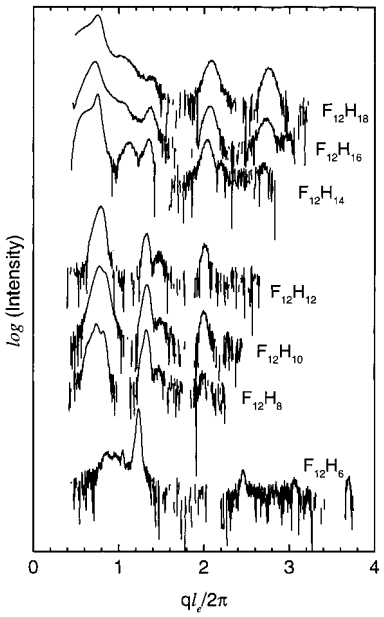

Figure 5. Low-temperature SAXS profiles of all $F_{12}H_n$ samples at room temperature plotted as log(intensity) vs scattering vector normalized by the respective molecule length. In this representation the general shape of the curves can be compared more easily. The individual data are shifted vertically for clarity.

We will now discuss the spectra in detail and will finally suggest a model for the molecular packing of the semifluorinated alkanes with $n \le 12$. The SAXS curve from the $F_{12}H_6$ sample at 25 °C is displayed in Figure 6. The main feature of this spectrum is a triplet of equidistant peaks at $q = 3$, 6, and 9 nm^{-1}, which is clear evidence for a lamellar structure of the sample. The minor peak at $q = 2.44$ nm^{-1} left of the most intense first-order peak from these lamellar stacks is due to a remainder of the high-temperature phase at ambient temperature. The d spacing of the lamellar structure is calculated according to Bragg's law to be $d_{Bragg} = 2\pi/q = 2.09$ nm which is about 80% of the extended chain length of a $F_{12}H_6$ molecule. It is therefore very likely that the lamellae consist of monolayers of tilted $F_{12}H_6$ molecules. Assuming an extended configuration of the molecules and a uniform tilt direction for both molecular moieties, a tilt angle of $\phi = \arccos(d_{Bragg}/l_e) = 35.6°$ is calculated. It is conceivable as well that the fluorinated and hydrogenated parts have different tilt angles, as both moieties have different cross-sectional areas and consequently different lateral spatial requirements. However, it is not possible to judge from the present small-angle data which one of these pictures is correct.

Apparently the SAXS curves from the samples with $8 \le n \le 12$ are more complicated. In Figure 7 the data

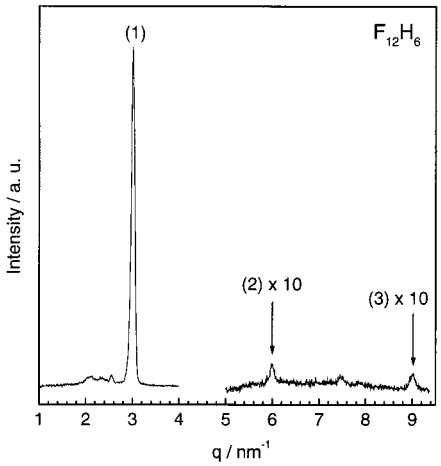

Figure 6. SAXS data diagram of the $F_{12}H_6$ compound at room temperature. The two unmarked peaks are reminiscent of the high-temperature phase, and the marked peaks are exactly equally spaced on the abscissa. Note that the right spectrum is multiplied by a factor of 10.

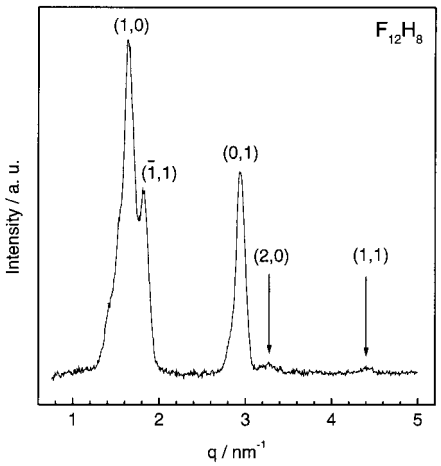

Figure 7. SAXS profile of the $F_{12}H_8$ sample at room temperature. The pattern of Miller indices is based on a two−dimensional oblique unit cell (see also Figure 8).

from the $F_{12}H_8$ sample at 30 °C are plotted as a representative for the entire group. This spectrum consists of five Bragg peaks, and it is remarkable that only one pair meets the higher order scattering condition; i.e., the very weak reflex at $q = 3.30$ nm^{-1} is second-order to the most intense one at $q = 1.64$ nm^{-1}. This means that the samples do not have a simple lamellar—be it monolayered or double-layered—structure as was suggested earlier.[10,11] As the Bragg peaks occur up to a maximum scattering vector of $q \approx 4.4$ nm^{-1} corresponding to a minimal length of about 1.4 nm, it is evident that there exists a superlattice with a typical length scale which lies in the range of the length of the molecules. Such a superstructure was suggested earlier by Dorset[22] based on electron diffraction measurements. It was pointed out that this finding is not compatible with the structures proposed by Rabolt et al. and Russell et al.

It is likely that such a superstructure has a fairly low symmetry; i.e., at worst a triclinic unit cell. However, we could not find a pattern of Miller indexing for the five peaks consistent with a three-dimensional monoclinic unit cell. Further observations made in atomic force microscopy demonstrate that all samples obviously have some kind of layered structure.[23] We therefore

Table 2. Peak Positions and Corresponding Lattice Parameters According to the Model of a Two-Dimensional Oblique-Angled Unit Cell

sample	$q_{1,0}$, nm^{-1}	$q_{-1,1}$, nm^{-1}	$q_{0,1}$, nm^{-1}	$q_{2,0}$, nm^{-1}	$q_{1,1}$, nm^{-1}	a, nm	b, nm	γ, deg
$F_{12}H_8$	1.64	1.83	2.94	3.3	4.41	6.85	3.83	146
$F_{12}H_{10}$	1.58	1.74	2.72	3.1	4.08	6.60	3.83	143
$F_{12}H_{12}$	1.46	1.51	2.49	2.8	3.79	7.81	4.57	147

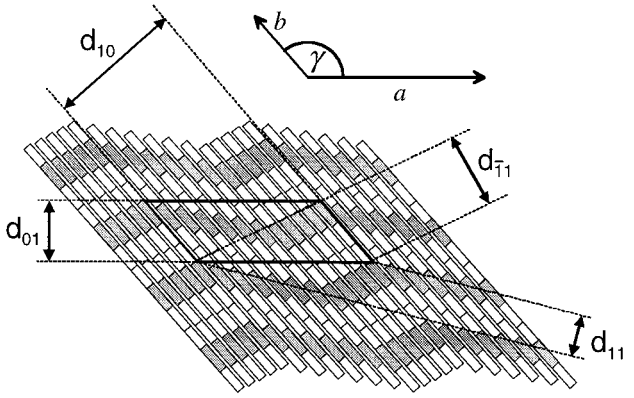

Figure 8. Proposed molecular packing and corresponding two−dimensional oblique unit cell perpendicular to the layer planes in the low-temperature phase of $F_{12}H_n$ samples. Shaded areas represent fluorinated segments, and white areas represent hydrocarbon chains. The figure is not drawn to scale.

suggest that the observed SAXS pattern originates from a two-dimensional lattice perpendicular to the plane of the observed layers. A probable periodicity within these layer planes is beyond the spatial resolution of our experiment. Consequently, the two-dimensional unit cell has to be oblique in order to cause the observed number of SAXS peaks. For such a unit cell the relation between the lattice parameters a, b, and γ, the Miller indices h and k, and the positions of the Bragg peaks $q_{h,k}$ reads[24]

$$q_{h,k} = \frac{2\pi}{\sin\gamma}\sqrt{\frac{h^2}{a^2} + \frac{k^2}{b^2} - \frac{2hk}{ab}\cos\gamma} \qquad (5)$$

Actually it is possible to index the SAXS pattern consistently with eq 5. The positions of the Bragg peaks and the corresponding lattice parameters according to this model are collected in Table 2 for the samples with $8 \le n \le 12$. From these data it is evident that the unit cell in all three cases is characterized by approximately the same angle $\gamma = 145°$ and that in all cases the lattice constants are significantly larger than the length of an extended $F_{12}H_n$ molecule. The latter point has to be accounted for in a molecular model for the packing of the $F_{12}H_n$. As Russell et al. pointed out, the d spacing which corresponds to the $q_{1,0}$ peak is proportional to twice the length of an F_{12} chain plus the all−trans length of the hydrocarbon chains for the samples with $8 \le n \le 12$. Thus, a double-layered structure with interdigitating hydrocarbon chains and a finite tilt angle appears to be a possible arrangement.

However, to give rise to the observed scattering pattern, these layers must not be flat; they rather have to be undulated as sketched in Figure 8. In this arrangement neighboring molecules are somewhat displaced along their long axes. A stack of flat layers would give rise to a simple SAXS pattern of equidistant peaks independent of the arrangement of the molecular entities within the layer, as is observed for $F_{12}H_6$ and in

the high-temperature phases. On the other hand, a stack of undulating lamellae is characterized by an oblique two−dimensional unit cell, similar to lyotropic liquid-crystalline "ripple phases" in lecithin bilayers.[25] The reason for the displacement of the molecules along their long axes may be due to the helical structure of the F_{12} groups: the spatial arrangement is favorable if ridges and valleys of right- and left-handed helices face each other.[26] As discussed already for the $F_{12}H_6$ sample, it is not necessary that the fluorinated and hydrogenated moieties have the same tilt angle, but this question has to be left to detailed wide-angle diffraction measurements.

The WAXD experiments we performed on these samples in the low-temperature phase nicely confirm the spectra published by Rabolt et al., who already pointed out that a quantitative interpretation of data at this level of resolution is not possible. On a qualitative level we can say that in this low-temperature phase the molecules are no longer in a hexagonal rotator phase because in the WAXD spectra 7−10 peaks in the *d* spacing range of 0.40−0.55 nm can be observed. Further experiments on single crystals are therefore necessary to solve the complete structure.

Conclusion

In this contribution we have reinvestigated the X-ray scattering from pure $F_{12}H_n$ powder samples. We have reproduced the basic features of the data presented earlier by Rabolt et al. and Russell et al., and we were able to add some detailed information on the molecular packing of these samples. This was possible since we used a point-collimated incident X-ray beam for our experiments in contrast to the above authors. Consequently, we obtained details of the scattering curves which had been buried by data smearing caused by the beam profile applied in the former experiments. In the so−called high-temperature phase we find, in accordance with earlier reports, that all samples have a lamellar structure, consisting of stacked monolayers of $F_{12}H_n$ molecules in a rotator phase. However, differently from former contributions we find that the F_{12} segments are very likely to stand upright on the lamellar plane. Additionally, we found that the number of layers which contribute coherently to the scattering is limited to about 30−40 layers, which shows that the samples are only weakly ordered; i.e., they exhibit liquid-crystalline character rather than crystalline. For the $F_{12}H_6$ sample we find a monolayered lamellar structure also in the low-temperature phase where the molecular axes are tilted with respect to the layer normal. In the case of the samples with $8 \leq n \leq 12$, the structure appears to consist of double-layered undulating lamellae with interdigitating hydrocarbon chains. This structure may be regarded as an improvement of the model suggested earlier in two respects: First, the oblique unit cell accounts for the rather complex appearance of the SAXS spectra while the structure suggested by Rabolt et al. would lead to a pattern of equidistant Bragg peaks. Second, the amount of contacts between fluorinated and hydrogenated segments is kept at a minimum level in the presently suggested structure. However, there still remains a number of important questions to be answered. For instance, we could not further enlighten the structure of the samples with $n \geq 14$. Further, we do not know whether the hydrocarbon and fluorocarbon segments have the same tilt angle, a question which is directly related to the problem of the lateral arrangement of the F_mH_n molecules within the layers. All of these questions have to be left to detailed wide-angle diffraction experiments.

Acknowledgment. We thank E. Lermann for preparation of the $F_{12}H_n$ samples and M. Möller and R. Steitz for helpful discussions. Financial support by the Sonderforschungsbereich 335/Teilprojekt A8 of the Deutsche Forschungsgemeinschaft is gratefully acknowledged. We also thank the reviewers for pointing our attention to some interesting literature[25] concerning ripple phases in phospholipid research.

References and Notes

(1) Dunlap, R. D.; Bedford, R. G.; Woodbrey, J. C.; Furrow, S. D. *J. Am. Chem. Soc.* **1959**, *81*, 2927.
(2) Christensen, J. J.; et al. *Handbook of Heats of Mixing*; Wiley: New York, 1982.
(3) Mahler, W.; Guillon, D.; Skoulios, A. *Mol. Cryst. Liq. Cryst. Lett.* **1985**, *2*, 111.
(4) Viney, C.; Russell, T. P.; Depero, L. E.; Twieg, R. J. *Mol. Cryst. Liq. Cryst.* **1989**, *168*, 63.
(5) Viney, C.; Twieg, R. J.; Russell, T. P.; Depero, L. E. *Liq. Cryst.* **1989**, *5*, 1783.
(6) Binks, B. P.; Fletcher, P. D. I.; Sager, W. F. C.; Thompson, R. L. *Langmuir* **1995**, *11*, 977.
(7) Hayami, Y.; Findenegg, G. H. *Langmuir* **1997**, *13*, 4865.
(8) Turberg, M. P.; Brady, J. E. *J. Am. Chem. Soc.* **1988**, *110*, 7797.
(9) Binks, B. P.; Fletcher, P. D. I.; Thompson, R. L. *Ber. Bunsen-Ges. Phys. Chem.* **1996**, *100*, 232.
(10) Rabolt, J. F.; Russell, T. P.; Twieg, R. J. *Macromolecules* **1984**, *17*, 2786.
(11) Russell, T. P.; Rabolt, J. F.; Twieg, R. J.; Siemens, R. L.; Farmer, B. L. *Macromolecules* **1986**, *19*, 1135.
(12) Viney, C.; Twieg, R. J.; Russell, T. P. *Mol. Cryst. Liq. Cryst.* **1990**, *182B*, 291.
(13) Höpken, J.; Pugh, C.; Richtering, W.; Möller, M. *Makromol. Chem.* **1990**, *189*, 911.
(14) Höpken, J. Ph.D. Thesis, University of Twente, The Netherlands, 1991.
(15) Huang, T. C.; Toraya, H.; Blanton, T. N.; Wu, Y. *J. Appl. Crystallogr.* **1993**, *26*, 180.
(16) Lo Nostro, P.; Chen, S.-H. *J. Phys. Chem.* **1993**, *97*, 6535.
(17) Tanford, C. *The Hydrophobic Effect*; Wiley: New York, 1973.
(18) Bunn, C.W.; Howell, E. R. *Nature* **1954**, *174*, 549.
(19) Strobl, G. R.; Schwickert, H.; Trzebiatowski, T. *Ber. Bunsen-Ges. Phys. Chem.* **1983**, *87*, 274.
(20) Strobl, G. R.; Ewen, B.; Fischer, E. W.; Piesczek, W. *J. Chem. Phys.* **1974**, *61*, 5257.
(21) Schwickert, H.; Strobl, G. R.; Kimmig, M. *J. Chem. Phys.* **1991**, *95*, 2800.
(22) Dorset, D. L. *Macromolecules* **1990**, *23*, 894.
(23) Lermann, E. Ph.D. Thesis, University of Ulm, Ulm, Germany, 1997.
(24) Buerger, M. J. *X-Ray Crystallography*; Wiley: New York, 1962.
(25) For example, see: Sun, W.-J.; Tristram-Nagle, S.; Suter, R. M.; Nagle, J. F. *Proc. Natl. Acad. Sci. U.S.A.* **1996**, *93*, 7008.
(26) Strobl, G. R.; Stühn, B.; Schwickert, H.; Ritter, C. *J. Chem. Phys.* **1991**, *95*, 2807.

MA981130J